Available online at www.sciencedirect.com
SCIENCE DIRECT®
ELSEVIER
Earth and Planetary Science Letters 221 (2004) 263–273
EPSL
www.elsevier.com/locate/epsl

# High sensitivity of ocean ridge thermal structure to changes in magma supply: the Galápagos Spreading Center

Yongshun John Chen [a], Jian Lin [b,*]

[a] *Computational Geodynamics Laboratory, Department of Geophysics, School of Earth and Space Sciences, Peking University, Beijing 100871, PR China*

[b] *Department of Geology and Geophysics, Woods Hole Oceanographic Institution, Woods Hole, MA 02543, USA*

Received 16 June 2003; received in revised form 27 January 2004; accepted 29 January 2004

**Abstract**

We explore the physical mechanisms for the observed apparent sensitivity of ridge axis topography and crustal magma systems to small changes in magma supply at intermediate spreading rates. Numerical experiments were carried out to simulate crustal temperature structure of the Galápagos Spreading Center, which spreads at intermediate spreading rates with its various sections appear to have been influenced to different degrees by the nearby Galápagos hotspot. Model results show a strong 'threshold' effect: as the crustal thickness decreases from 7.4 km at the 92°W area with an axial high westward to 6.0 km at the 94°W area with a transitional topography, the depth to the top of a magma lens is calculated to increase from 1.7 to 2.5 km. In contrast, at the 97°W area, where crustal thickness is only 5.6 km and a rift valley is present, the model results predict no steady-state magma lens in the crust. These model calculations provide a simple physical explanation for the recent observations along the Galápagos Spreading Center, where abrupt changes in both magma lens and axial morphology occur within a short distance but crustal thickness changes only modestly. Results of this investigation illustrate the critical importance of hotspots in influencing mid-ocean ridge crustal thickness and the associated changes in thermal structure, especially for ridges that spread at the sensitive range of intermediate spreading rates.


*Keywords:* mid-ocean ridges; hotspot–ridge interaction; hydrothermal cooling; crustal thermal structure; depth of magma lens; Galápagos

## 1. Introduction

The Galápagos is a classic example of an interactive hotspot–ridge system [1–3]. The influence of the Galápagos hotspot on the nearby Galápagos Spreading Center (GSC) can be readily observed in along-axis variations in bathymetry, gravity, geochemical anomalies, as well as in the off-axis relicts of seafloor depth and residual gravity anomalies [2,4–12].

Previous studies have shown that at intermediate spreading rates, the calculated depth to the top of a steady-state magma lens increases sharply with decreasing spreading rate, and thus even a

* Corresponding author. Tel.: +1-508-289-2576; Fax: +1-508-457-2187.
*E-mail addresses:* johnyc@pku.edu.cn (Y.J. Chen), jlin@whoi.edu (J. Lin).

0012-821X/04/$ – see front matter © 2004 Elsevier B.V. All rights reserved.
doi:10.1016/S0012-821X(04)00099-8

small perturbation in mantle temperature could cause thermal re-equilibrium of the system in a relatively significant way [13–14]. Spreading at intermediate half spreading rates of 20–30 mm/yr, the GSC is, therefore, expected to be very sensitive to small changes in magma supply. As is in the case of the slow-spreading Reykjanes Ridge–Iceland system, the influence of the Galápagos

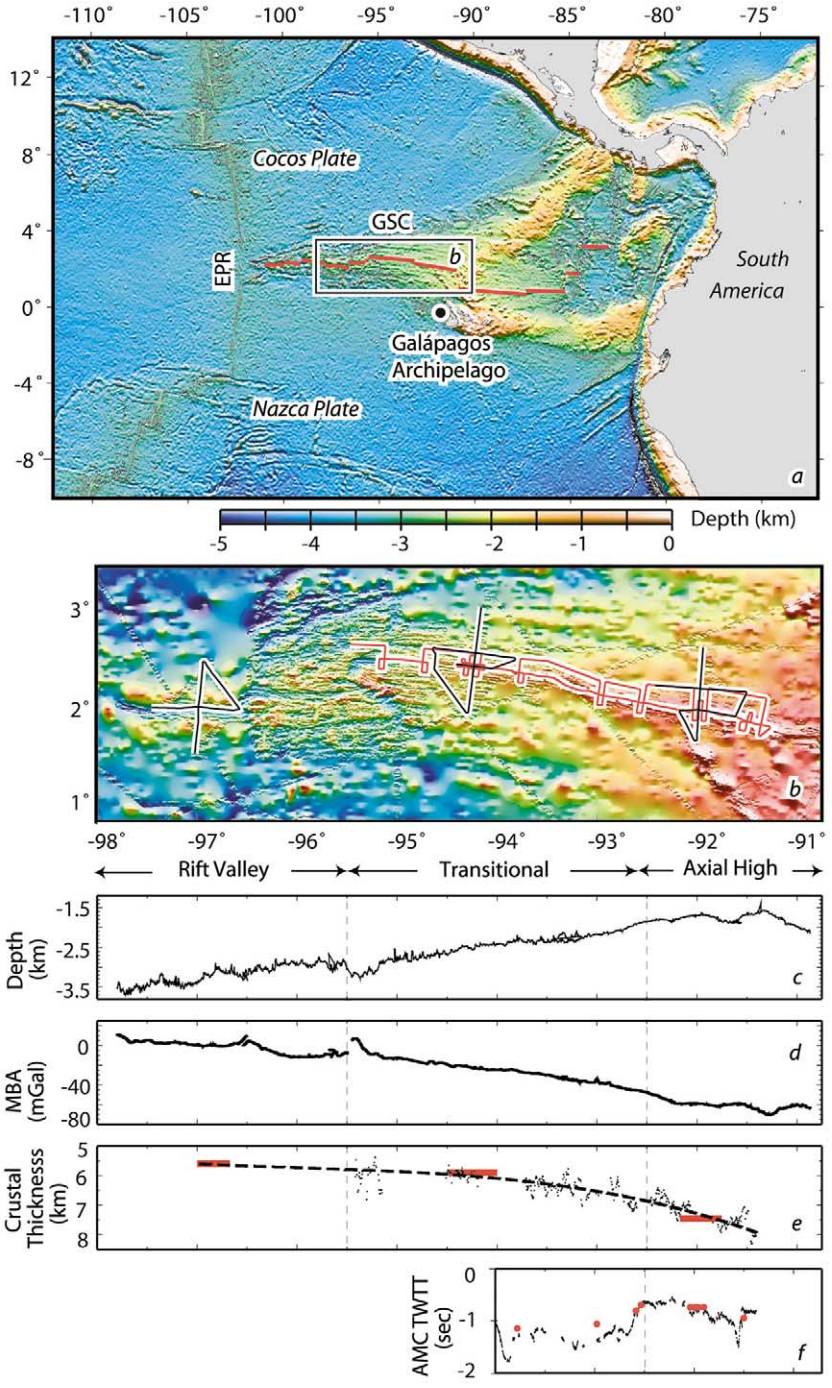

hotspot on crustal accretion processes at the GSC should be significant, despite its distance off the ridge axis, making it an excellent place to investigate ridge–hotspot interaction.

In this study we carry out a set of numerical experiments to investigate how changes in magma supply influence the thermal structure of the GSC. Our investigation focuses on three sections of the GSC at 92°W, 94°W, and 97°W, respectively, where recent seismic experiments have obtained constraints on both crustal thickness and depth to the top of magma lens. Such high-quality observations provide an unprecedented opportunity to investigate the sensitivity of ridge thermal structure to small changes in magma supply at intermediate spreading rates.

## 2. Recent constraints from the CSC

A regional bathymetric swell extends for more than a thousand kilometers along the GSC (Fig. 1a) with the peak axial bathymetry near 91°W, which is ~200 km north of the proposed center of the Galápagos mantle plume [15–16]. Correspondingly, regional mantle–Bouguer gravity anomaly (MBA) becomes increasingly negative along the GSC with a minimum (~90 mGal) at 91°W [10]. These along-axis variations in both bathymetry and gravity roughly correspond to the overall trends in $Sr^{87}/Sr^{86}$ and other isotopic anomalies in ridge-axis basalt samples (e.g. [2]). The ridge axis discontinuities in the study area are relatively small in their age offset and thus their effects on ridge thermal structure are probably local rather than regional (e.g. [12]).

A seismic experiment was conducted along the GSC between 91°W and 98°W in 2000 on board R/V *Ewing*, and a follow-up cruise collected basalt samples at a relatively close spacing [17]. Seismic refraction experiments were carried out at three locations on the GSC near 92°W, 94°W, and 97°W, using ocean bottom seismometer deployment and air gun acoustic sources (Fig. 1b). Multi-channel seismic reflection (MCS) data were also collected nearly continuously along the GSC axis from 91.2°W to 95°W, as well as along a ridge-parallel profile north of the ridge axis (Fig. 1b). These long ridge-parallel profiles were tied together by short across-axis profiles at several locations. The MCS data were collected using a 6-km-long seismic steamer [17]. Details of seismic data processing are given in references [12,17].

The seafloor depth of the ridge axis shoals by almost 2 km, from ~3.5 km near 98°W to only 1.5 km at 91.2°W (Fig. 1c). Correspondingly, the MBA changes by about 80 mGal, from about 10 mGal near 98°W to −70 mGal near 91.2°W (Fig. 1d). Seismic refraction data indicate crustal thickness of 5.6–6 km in the vicinity of the 97°W experimental site, which is associated with a rift valley (Fig. 1e). In the transitional region between 95°W and 92.7°W, the axial morphology is neither an axial valley nor an axial high, and the crustal thickness is in the range of 6–7 km. Meanwhile, the crustal thickness is 7–8 km in the region between 92.7°W and 91.5°W, which is characterized by an axial high (Fig. 1e). Within the transitional region, the top of an axial magma chamber (AMC) is at a depth of 2.5–4.25 km, corresponding to two-way travel time (TWTT) of 1.0–1.7 s

←

Fig. 1. (a) Map of predicted bathymetry based on data of Smith and Sandwell [28]. Abbreviations: GSC, Galápagos Spreading Center; EPR, East Pacific Rise. The black/white bull's eye circle marks the inferred center of the Galápagos mantle plume. Location of (b) is marked by the black box. Color scale applies only to (a). (b) Bathymetry of the GSC at 90.8–98°W. The ridge-axis morphology changes from an axial high east of 92.5°W to a rift valley west of 95.5°W. Black lines show seismic refraction lines in OBS/water gun experiments, and red lines show multi-channel seismic reflection (MCS) profiles [12,17]. (c) Along-axis depth profile along the GSC axis. (d) Mantle Bouguer anomaly (MBA) along the GSC. (e) Crustal thickness as measured by seismic refraction experiments (red bars) and as interpreted from the MCS data (black dots). Dashed curve shows a smooth fit to the MCS data. (f) Two-way-travel time (TWTT) to a seismic reflector that is interpreted as the top of an axial magma chamber (AMC). Shown are data from the along-axis (black dots) and across-axis (red circles) profiles. (b–f) are reproduced from Detrick et al. [17].

(Fig. 1f). The top of the AMC is considerably shallower (1.38–2.25 km or TWTT of 0.55–0.9 s) in the axial high region between 91.5°W and 92.7°W [12,17].

One important observation worthy of special mention is that the changes in the axial morphology and depth to AMC are quite abrupt along the ridge axis. Near 92.7°W, for example, an axial high develops within a short distance of only 20 km, with corresponding shoaling of the depth to AMC by as much as 1 km (Fig. 1) [17]. These observations suggest that axial morphology might be closely linked to the character of AMC beneath the seafloor, and both could be very sensitive to small changes in magma supply of a ridge.

## 3. Model parameterization

Our model [18] predicts that the interplay between the heat input to the base of the crust from magma supply and the heat loss from the seafloor via hydrothermal cooling controls the thermal equilibrium of the crust (Fig. 2), which in turn influences ridge axis topography through its effects on the rheological properties and deformation patterns of the young oceanic lithosphere [13,14,24–26]. The magma supply is represented by the potential mantle temperature, $T_m$, in our model (Fig. 2). The model is assumed to be 2-D and steady-state with much finer numerical grid spacing in both the horizontal and vertical directions near the ridge axis and in the crust and

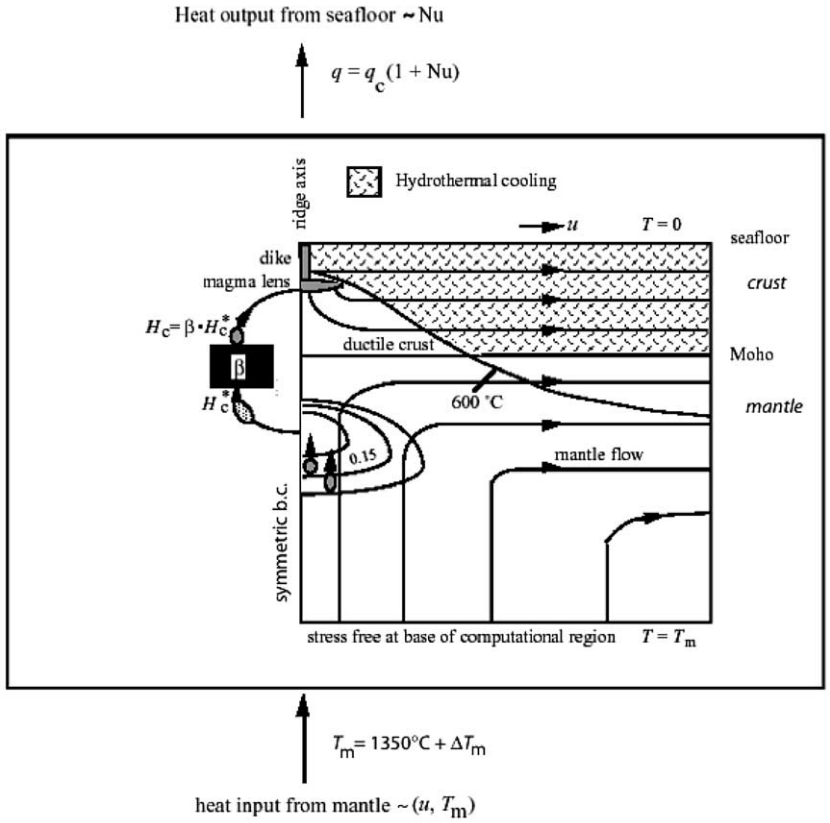


Fig. 2. Sketch of key factors controlling thermal equilibrium at mid-ocean ridges [18]. Magma supply is controlled by potential mantle temperature, $T_m$, and half spreading rate, $u$. Steady-state temperature field near the ridge axis is determined by thermal equilibrium between heat conduction and advection, release of latent heat as melt solidifies in a vertical narrow dike zone and a horizontal magma lens, and hydrothermal circulation, represented here as enhanced thermal conductivity, in the shallow crust.

shallow mantle, where temperature fields have the greatest spatial gradients [18]. In each calculation the total melt production rate in the upwelling mantle is calculated from a numerical model for a passive spreading center [19]. Each combination of the assumed mantle temperature, $T_m$, and half spreading rate, $u$, yields a calculated maximum crustal thickness, $H_c$*, which equals the total melt production rate divided by the full spreading rate. A model parameter β is introduced to denote the fraction of the total melt produced in the upwelling mantle that eventually migrates to the crustal level to create the new oceanic crust, i.e., $H_c = \beta \cdot H_c$*, where $H_c$ is the crustal thickness. The remaining fraction of the melt that does not make to the crustal level, i.e., $(1-\beta)\cdot H_c$*, is assumed to have frozen in the upper mantle.

Seismic observations over the world's ocean basins indicated that, on average, the oceanic crust has more-or-less a constant thickness for half rates greater than 10 mm/yr (e.g. [20–22]), below which the average crustal thickness appears to decrease with spreading rate. Using this observation as a constraint, the value of β is adjusted in our model runs to produce a 6-km crust for a reference mantle temperature of 1350°C at a given spreading rate. This simplified approach yields a linear increase in crustal thickness with mantle temperature [18].

We envision that when the melt reaches the crustal level beneath the ridge axis, it is injected into a narrow vertical dike zone and a thin horizontal magma lens (Fig. 2) [13]. The crystallization temperature of the melt (here chosen to be 1200°C) determines the steady-state depth of the lens at the ridge axis. If the entire crust beneath the ridge axis is cooler than 1200°C, however, a steady-state magma lens is not permitted in the crust. In this case, melt solidification in the narrow vertical dike zone is assumed to be the only mode of crustal accretion.

Hydrothermal cooling is treated as an enhanced thermal conductivity, $K_c$*, within the crustal region penetrated by seawater circulation, which is assumed to occur within the cold and brittle crust ($< 600$°C). Here the enhanced thermal conductivity is parameterized by $K_c$* = Nu·$K_c$, where $K_c$ is the actual thermal conductivity of the crust and Nu is the Nusselt number of hydrothermal circulation defined as the ratio of convective to conductive heat transfer in a hydrothermal convection system.

We solve simultaneously the momentum balance equation that governs the flow field and the thermal equilibrium equation that describes steady-state heat balance in a model box centered at the ridge axis with appropriate boundary conditions. The computational method, model grid spacing, and methods of obtaining numerical solutions are described in detail in an early study [18].

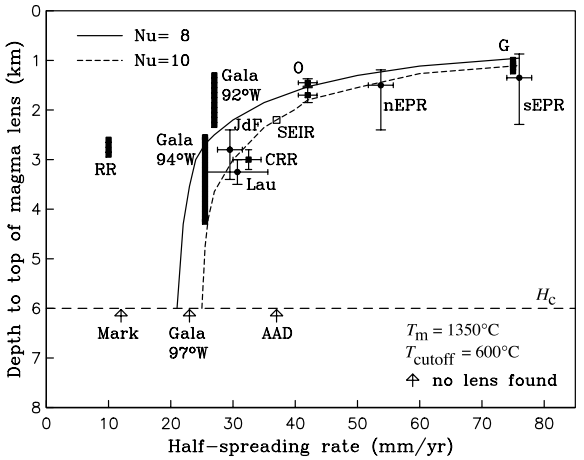


Fig. 3. The calculated depth to top of magma lens (defined as depth of the 1200°C isothermal at the ridge axis) for a reference mantle temperature $T_m = 1350°$ as a function of spreading rate, together with seismic observations [18]. The enhanced heat conduction due to hydrothermal circulation is assumed to occur only in the crust where the temperature is less than the $T_{cutoff}$. The two curves show the results of a suite of numerical experiments with Nu = 8 (solid line) and 10 (dotted line), respectively, while all other parameters are held constant. Data sources: G, East Pacific Rise south of the Garrett transform [29]; O, East Pacific Rise north of Orozco transform [30]; SEIR, Southeast Indian Ridge [31]; CRR, Costa Rica Rift [32]; RR, Reykjanes Ridge [33]; AAD, Australia–Antarctica Discordance [31]; MARK, Mid-Atlantic Ridge at the Kane Fracture Zone [34]; Jdf, Juan de Fuca Ridge [35,36]; Lau, Lau Basin [37]; sEPR and nEPR, southern and northern East Pacific Rise, respectively [38,39]. Gala 92°W and Gala 94°W represent the ranges of the AMC depth observed at 91.5–92.7°W and 92.7–95°W, respectively, along the GSC; no AMC is detected at the GSC 97°W area [12,17].

## 4. Results

As an illustration of the influence of spreading rate and hydrothermal cooling, Fig. 3 shows the calculated depth to top of the magma lens (defined as the depth of the 1200°C isotherm beneath the ridge axis) for a reference mantle temperature of $T_m = 1350$°C and Nu = 8 (dashed line) and Nu = 10 (solid line), respectively. The predicted trend matches the seismic observations quite well: the magma lens deepens from ~1–1.8 km at fast ridges (40–75 mm/yr) to ~2.2–3.5 km at intermediate ridges (~30 mm/yr). Data for the three GSC locations with good seismic constraints are also shown in Fig. 3. It is apparent that GSC is within the sensitive range of intermediate spreading rates, where models predict a sharp transition from a deep lens at 30 mm/yr to no lens < 20 mm/yr, even if the mantle temperature $T_m$ and the corresponding crustal thickness are assumed to remain a constant.

We next calculate the mantle temperature anomalies, $\Delta T_m$ (where $T_m = 1350$°C+$\Delta T_m$) that are required to produce the observed crustal thickness at each of the three GSC locations, 92°W, 94°W, and 97°W, for which there are seismic refraction measurements. The resulting temperature and velocity fields within the crust are shown in Fig. 4. In these calculations, the Nusselt number, Nu, which simulates the effect of hydrothermal cooling, is kept constant in order to isolate the effects of other parameters. In our model the mantle temperature influences the thermal system of the crust and shallow mantle mostly through its effects on the calculated crustal thickness that represents the magma supply.

At 97°W, where the GSC spreads at a half-rate of 23 mm/yr and the ridge axis is characterized by a rift valley, the observed Moho is at a depth of 5.6 km beneath the seafloor [12]. Reproducing the observed crustal thickness of 5.6 km here requires a negative mantle temperature anomaly $\Delta T_m = -10$°C (Fig. 4a). Within the crust the calculated temperature is mostly below 600°C except in a small region in the lower crust right beneath the ridge axis, where temperature exceeds 1000°C with the potential to allow partial melt to be present. But the calculated crustal thermal structure for

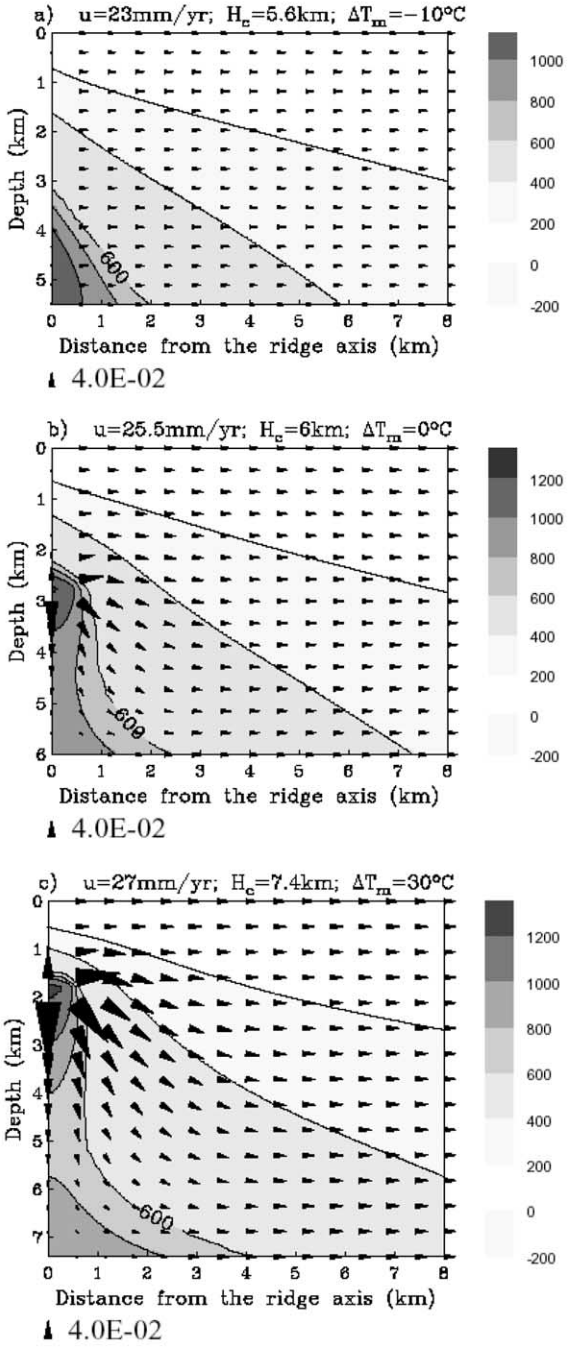


Fig. 4. The calculated temperature and flow fields within the crust at the three GSC locations where seismic constraints are available. (a) GSC at 97°W with half-spreading rate of 23 mm/yr. (b) GSC at 94°W, half rate of 25.5 mm/yr. (c) GSC at 92°W, half rate of 27 mm/yr.

this ridge section is too cold to host a steady-state magma lens in the crust, which is consistent with the observation that an AMC reflector was not identified west of 95°W at the GSC [17].

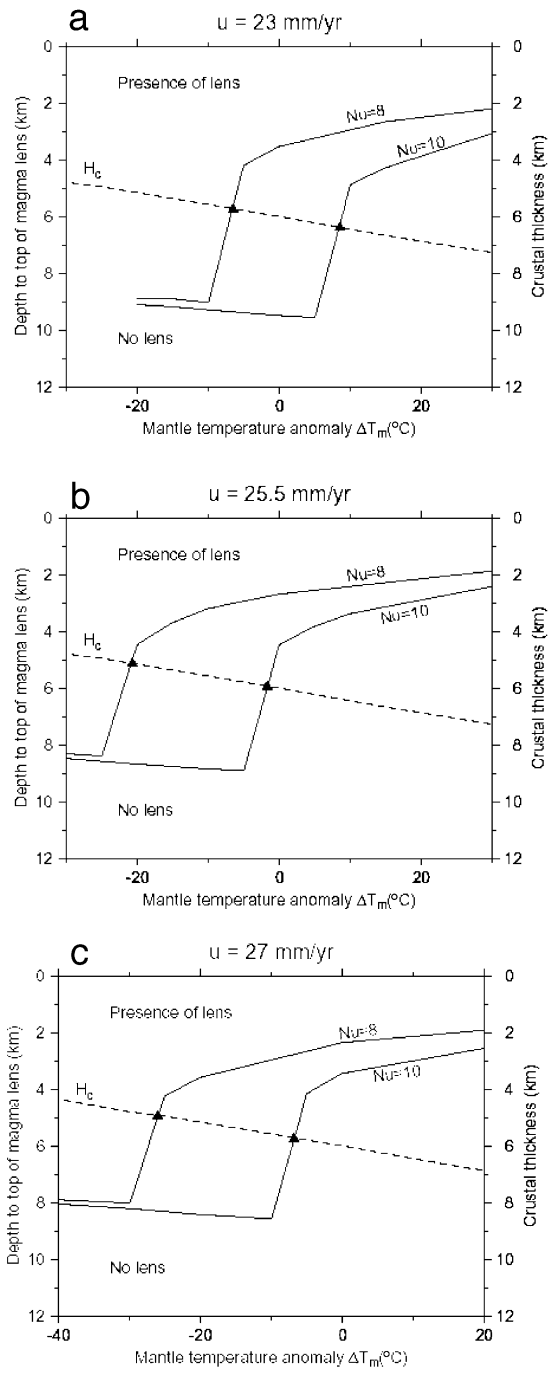


On the high magma supply section at 92°W, the GSC is spreading at a slightly higher half-rate of 27 mm/yr with seismic crustal thickness of 7.4 km and an axial topographic high [12]. Fig. 4c shows the calculated temperature field with an excess mantle temperature $\Delta T_m = 30$°C that can produce enough magma supply to make the 7.4-km crust. The calculated depth to the 1200°C at the ridge axis is at 1.7 km, similar to the depth to the top of the AMC observed in this area. The resulting thermal structure is very similar to that of a fast spreading ridge ($>40$ mm/yr) [18], even though the half-spreading rate here is only 27 mm/yr. Therefore, the observation of an axial high at this section of the GSC should not be a surprise at all: it has the characteristics of a fast spreading ridge including thermal structure and shallow magma lens, except that here it is due to the near-by Galápagos hotspot producing a higher magma supply and thicker crust.

At 94°W, the GSC axial topography is transitional, displaying neither an axial valley nor a topographic high. The crustal thickness here ($\sim$6 km) is very close to the global average [20–22]. The calculated depth to the 1200°C at the ridge axis is at 2.5 km, again within the range of the observed AMC depth in this area. The calculated temperature field (Fig. 4b) is typical for an intermediate spreading-rate ridge with a magma lens at the mid-crustal level ($3 \pm 0.5$ km). Comparison of results in Fig. 4 shows that ridge-axis thermal structure is very sensitive to small changes in magma supply at the intermediate spreading rates corresponding to the GSC.

To investigate the combined effects of mantle temperature variations and hydrothermal cooling,

←

Fig. 5. The calculated depth to top of magma lens (defined as depth of the 1200°C isothermal at the ridge axis) (left axis) and the calculated crustal thickness (right axis) as a function of mantle temperature anomaly (bottom axis) for three different half-spreading rates ($u = 23$, 25.5, and 27 mm/yr) and two Nusselt numbers (Nu = 8 and 10). Note a 'threshold' mantle temperature above which small changes in mantle temperature can cause dramatic change in axial thermal structure, resulting in a sharp transition from the presence of a magma lens to absence of such a lens in the crust.

a set of calculations was conducted for a range of mantle temperature anomaly $\Delta T_m$ and Nu number values of 8 and 10, respectively, for each of the three GSC locations (Fig. 5). Here again the depth to a magma lens is determined by the location of the 1200°C isotherm within the crust at the ridge axis. When a magma lens is not present in the crust, the depth to the 1200°C isothermal in the mantle is instead plotted in Fig. 5, which is a simplified way to denote the absence of a magma lens in the crust and does not imply a magma lens in the mantle. The predicted crustal thickness as a function of mantle temperature is also shown. Note that this calculated crustal thickness crosses 6 km at the reference mantle temperature, $\Delta T_m = 0$°C, as required by the choice of the β value.

These modeling results clearly show a 'threshold' effect in which small changes in mantle temperature can lead to significant changes in axial thermal structure and a sharp transition from the presence to absence of a magma lens in the crust. Such a 'threshold' effect arises because ridge-axis thermal structure at intermediate rates is only marginally sufficient for maintaining a steady-state magma lens, and thus any perturbations in the magma supply, and/or perturbations in the degree of hydrothermal cooling, could decide the fate of whether or not a steady-state magma lens can be maintained. This predicted 'threshold' effect (or sharp transition, which is also a function of spreading rate) is consistent with the observed variations in magma lens depth and axial morphology along the GSC [12,17] and the Southeast Indian Ridge [23].

In summary, model calculations predict that a shallow magma lens should exist along the GSC east of 92.5°W, where increased magma supply due to the influence of the nearby Galápagos hotspot had produced a thicker (> 6 km) crust. On the other hand, the ridge west of 95.5°W, where reduced magma supply had resulted a thinner (< 6 km) crust, is predicted not to have a magma lens within the crust: the crust is apparently too cold to host a steady-state magma lens within the crust. Although the GSC within the transitional zone between 95.5°W and 92.5°W could have a magma lens within the crust, it is at a much greater depth than the GSC east of 92.5°W, making it more sensitive to any local variations in either magma supply or hydrothermal cooling. Furthermore, the total range of our calculated mantle temperature anomalies (from −10°C at 97°W to 30°C at 92°W) are in general agreement with the calculated total mantle temperature anomaly of ~30°C for the Galápagos based on simpler 1-D melt calculations [12] and within the range of the inferred mantle temperature variations from geophysical data modeling [10,12].

## 5. Discussion

Modeling results in Fig. 5 suggest that thermal structure of the intermediate spreading ridges is governed by crustal accretion variables. The synthesized effects of three model parameters, i.e., $T_m$, $u$, and Nu, are shown in Fig. 6 and compared with observations at the three GSC locations. The two curves shown in Fig. 6 represent the values of the crustal thickness or mantle temperature anom-

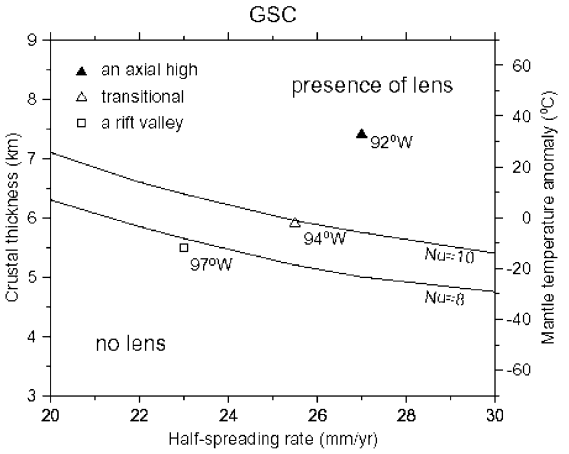


Fig. 6. Model results showing the transition from the presence to absence of a magma lens within the crust as a function of spreading rate (horizontal axis), curstal thickness (left axis), and mantle temperature anomaly (right axis). Data are from three locations of the GSC [17]: 92°W with an axial high morphology and a relatively shallow magma lens (filled triangle); 94°W with a rifted high or transitional morphology and a relatively deep magma lens (open triangle); 97°W with an axial valley and no magma lens (open square).

aly at the critical state that separates the presence and absence of a magma lens within the crust. The critical states are marked as filled triangles in Fig. 5 and are the intersections of the constant Nu curves and the linear function (dashed line) between crustal thickness and mantle temperature anomaly.

The good correlation between the predicted magma lens depth and the observed axial topography supports the notion that axial topography is directly linked to the thermal structure and thus the strength of the axial lithosphere [24–26]. The abrupt changes in both the observed depth to the magma lens and axial morphology at the GSC also support the hypothesis of a 'threshold' effect [13,25] at the intermediate spreading rates, in which small changes in magma supply can lead to significant changes in axial thermal structure, magma lens depth, and axial morphology as illustrated in this study (Fig. 5 and 6).

There are, of course, limitations of this rather simplified model, which cannot yet explain some features of the field observations. For example, there is clearly local variability in the AMC depth at the GSC 91.5–92.7°W section (Fig. 1f), where the TWTT changed by as much as 0.7 s. This significant change might be due to intra-segment spatial or temporal variability in magma supply similar to that reported for the southern East Pacific Rise [27]. Similarly, a sharp change in the AMC depth of ~0.4 s of TWTT is reported between 92.7°W and 91.5°W, implying as much as 1 km of change to the top of the magma lens within a short distance of less than 20 km. Future studies should investigate whether the observed sharp changes are caused by spatial or/and temporal changes in local magma supply and should examine the potential role of faulting, and thus enhanced hydrothermal circulation, in controlling local variability. Furthermore, the effect of mantle temperature in our modeling is to regulate the magma supply to the crustal accretion. If lateral variations in mantle composition can produce the systematic changes in magma supply reflected in the crustal thickness variations, then the conclusions of the threshold-type sensitivity reported in this study could similarly be applied.

## 6. Conclusions

We have carried out a set of numerical experiments to investigate the thermal equilibrium of the GSC, which spreads at intermediate half rates of 20–30 mm/yr while its various sections appear to have been influenced to different degrees by the nearby Galápagos hotspot. Model results reveal that the ridge thermal structure here is highly sensitive to small changes in magma supply:

- At the 92°W area, where the observed crustal thickness is 7.4 km and an axial high is present, the calculated depth to the top of a magma lens is 1.7 km. The magma lens depth is predicted to increase westward to 2.5 km at the 94°W area, where the measured crustal thickness is 6.0 km and the axial topography is transitional between an axial high and rift valley.
- In contrast, at the 97°W area where the crustal thickness is only 5.6 km and a rift valley is present, the model results predict no steady-state magma lens in the crust.

These results provide a simple physical explanation for the recent observations along the GSC, where abrupt changes in both magma lens depth and axial morphology occur within a short distance but crustal thickness changes only modestly. They also illustrate the critical importance of hotspots in influencing the crustal thickness and the associated changes in the thermal structure of mid-ocean ridges, especially at the sensitive range of the intermediate spreading rates.

## Acknowledgements

We are grateful to Jennifer Georgen for creating a draft version of Fig. 1a, Bob Detrick and Pablo Canales for providing preprints of their work on GSC, and X.-F. Chen for constructive review of an early version of this manuscript. Reviews by Alistair Harding, Dan Scheirer, and an anonymous referee helped improving the manuscript. Y.J.C. is supported by NSF of China Grant 40125011 and the Peking University, China. J.L. is supported by US NSF Grant OCE-9819117 and the Andrew W. Mellon Foundation Endowed Fund for Innovative Research at

WHOI. This is Woods Hole Oceanographic Institution Contribution Number 11088.*[SK]*

## References


[1] W.J. Morgan, Rodrigues, Darwin, Amsterdam, ..., A second type of hotspot island, J. Geophys. Res. 83 (1978) 5355–5360.

[2] J.-G. Schilling, R.H. Kingsley, J.D. Devine, Galápagos hot spot-spreading center system 1. Spatial petrological and geochemical variations (83°W–101°W), J. Geophys. Res. 87 (1982) 5593–5610.

[3] G.T. Ito, J. Lin, Oceanic spreading center–hotspot interactions: Constraints from along-isochron bathymetric and gravity anomalies, Geology 23 (1995) 657–660.

[4] R. Hey, F.K. Duennebier, W.J. Morgan, Propagating rifts on mid-ocean ridges, J. Geophys. Res. 85 (1980) 3647–3658.

[5] R. Hey, M.C. Kleinrock, S.P. Miller, T.M. Atwater, R.C. Searle, Sea beam/deep-tow investigation on an active oceanic propagating rift system, Galápagos 95.5°W, J. Geophys. Res. 91 (1986) 3369–3393.

[6] D.M. Christie, J.M. Sinton, Evolution of abyssal lavas along propagating segments of the Galápagos Spreading Center, Earth Planet. Sci. Lett. 56 (1981) 321–335.

[7] D.M. Christie, J.M. Sinton, Major element constraints on melting, differentiation and mixing of magmas from the Galápagos 95.5°W propagating rift system, Contr. Mineral. Petrol. 94 (1986) 274–288.

[8] R.C. Searle, Location and segmentation of the Cocos–Nazca Spreading Centre West of 95°W, Mar. Geophys. Res. 11 (1989) 15–26.

[9] D.S. Wilson, R.N. Hey, History of rift propagation and magnetization intensity for the Cocos–Nazca spreading center, J. Geophys. Res. 100 (1995) 10041–10056.

[10] G.T. Ito, J. Lin, Mantle temperature anomalies along the present and paleoaxes of the Galápagos spreading center as inferred from gravity analyses, J. Geophys. Res. 100 (1995) 3733–3745.

[11] J.P. Canales, J.J. Danobeitia, R.S. Detrick, E.E.E. Hooft, R. Bartolome, D.F. Naar, Variations in axial morphology along the Galápagos spreading center and the influence of the Galápagos hotspot, J. Geophys. Res. 102 (1997) 27341–27354.

[12] J.P. Canales, G. Ito, R.S. Detrick, J. Sinton, Crustal thickness along the western Galápagos Spreading Center and the compensation of the Galápagos hotspot swell, Earth Planet. Sci. Lett. 203 (2002) 311–327.

[13] J. PhippsMorgan, Y.J. Chen, The genesis of oceanic crust: Magma injection, hydrothermal circulation, and crustal flow, J. Geophys. Res. 98 (1993) 6283–6297.

[14] J. Phipps Morgan, Y.J. Chen, Dependence of ridge-axis morphology on magma supply and spreading rate, Nature 364 (1993) 706–708.

[15] D.J. Geist, W.M. White, A.R. McBirney, Plume–asthenosphere mixing beneath the Galápagos archipelago, Nature 333 (1988) 657–660.

[16] W.M. White, A.R. McBirney, R.A. Duncan, Petrology and geochemistry of the Galápagos Islands: Portrait of a pathological mantle plume, J. Geophys. Res. 98 (1993) 19533–19563.

[17] R.S. Detrick, J.M. Sinton, G. Ito, J.P. Canales, M. Behn, T. Blacic, B. Cushman, J.E. Dixon, D.W. Graham, J.J. Mahoney, Correlated geophysical, geochemical, and volcanological manifestations of plume–ridge interaction along the Galápagos Spreading Center, Geochem. Geophys. Geosystem 3 (2002) 8501, doi:10.1029/2002GC000350.

[18] Y.J. Chen, Dependence of crustal accretion and ridge axis topography on spreading rate, mantle temperature, and hydrothermal cooling, in: Y. Dilek, E.M. Moores, D. Elthon, A. Nicolas (Eds.), Ophiolites and Oceanic Crust: New Insights from Field Studies and the Ocean Drilling Program, Boulder, Colorado, Geol. Soc. Am. Spec. Pap. 349 (2000) 161–179.

[19] Y.J. Chen, Constraints on the melt production rate beneath the mid-ocean ridges based on passive flow models, Pure Appl. Geophys. 146 (1996) 590–620.

[20] I. Reid, H.R. Jackson, Oceanic spreading rate and crustal thickness, Mar. Geophys. Res. 5 (1981) 165–172.

[21] Y.J. Chen, Oceanic crustal thickness versus spreading rate, Geophys. Res. Lett. 19 (1992) 753–756.

[22] R.S. White, D. McKenzie, R.K. O'Nions, Oceanic crustal thickness from seismic measurements and rare earth element inversions, J. Geophys. Res. 97 (1992) 19683–19715.

[23] J.R. Cochran, M. Tolstoy, S.M. Carbotte, J.M. Baran, J.S. Floyd, E. Rubio, B. Medvedev, Effect of changes in mantle temperature on melt supply and crustal accretion along the Southeast Indian Ridge (abstract), EOS Trans. AGU 83 (2002) F1327.

[24] J. Lin, E.M. Parmentier, Mechanisms of lithospheric extension at mid-ocean ridges, Geophys. J. 96 (1989) 1–22.

[25] Y. Chen, W.J. Morgan, A nonlinear rheology model for mid-ocean ridge axis topography, J. Geophys. Res. 95 (1990) 17583–17604.

[26] W.T. Shaw, J. Lin, Models of ocean ridge lithospheric deformation: Dependence on crustal thickness, spreading rate, and segmentation, J. Geophys. Res. 101 (1996) 17977–17993.

[27] E.E.E. Hooft, H. Schouten, R.S. Detrick, Constraining crustal emplacement processes from the variation of seismic layer 2A thickness at the East Pacific Rise, Earth Planet. Sci. Lett. 142 (1996) 289–310.

[28] W.H.F. Smith, D.T. Sandwell, Global seafloor topography from satellite altimetry and ship depth soundings, Science 277 (1997) 195–196.

[29] M. Tolstoy, A.J. Harding, J.A. Orcutt, Deepening of the axial magma chamber on the southern East Pacific Rise toward the Garrett Fracture Zone, J. Geophys. Res. 102 (1997) 3097–3108.

[30] S. Carbotte, C. Mutter, J. Mutter, G. Ponce-Correa, Influence of magma supply and spreading rate on crustal

magma bodies and emplacement of the extrusive layer Insights from the East Pacific Rise at lat 16°N, Geology 26 (1998) 455–458.
[31] M. Tolstoy, A.J. Harding, J.A. Orcutt, J. Phipps Morgan, A seismic refraction investigation of the Australian Antarctic Discordance and neighboring South East Indian Ridges: Preliminary results, EOS Trans. AGU 76 (1995) S275.
[32] C.Z. Mutter, Seismic and hydrosweep study of the western Costa Rica Rift, EOS Trans. AGU 76 (1995) F595.
[33] M.C. Sinha, D.A. Navin, L.M. MacGregor, S. Constable, C. Peirce, A. White, G. Heinson, M.A. Inglis, Evidence for accumulated melt beneath the slow-spreading Mid-Atlantic Ridge, Philos. Trans. R. Soc. A 355 (1997) 233–253.
[34] R.S. Detrick, J. Mutter, P. Buhl, Multichannel seismic data from the MARK area (Mid-Atlantic Ridge, 23°N): No evidence for a crustal magma chamber, Nature 347 (1990) 61–64.
[35] J.L. Morton, N.H. Sleep, W.R. Normark, D.H. Tomkins, Structure of the southern Juan de Fuca Ridge from seismic reflection records, J. Geophys. Res. 92 (1987) 11315–11326.
[36] K.M.M. Rohr, B. Milkereit, C.J. Yorath, Asymmetric deep crustal structure across the Juan de Fuca Ridge, Geology 16 (1988) 533–537.
[37] J. Collier, M. Sinha, Seismic images of a magma chamber beneath the Lau Basin back-arc spreading centre, Nature 346 (1990) 646–648.
[38] R.S. Detrick, P. Buhl, E. Vera, J. Mutter, J. Orcutt, J. Madsen, T. Brocher, Multi-channel seismic imaging of a crustal magma chamber along the East Pacific Rise, Nature 326 (1987) 35–41.
[39] G.M. Purdy, L.S.L. Kong, G.L. Christeson, S. Solomon, Relationship between spreading rate and the seismic structure of mid-ocean ridges, Nature 355 (1992) 815–817.